CGT: CLUSTERED GRAPH TRANSFORMER FOR URBAN SPATIO-TEMPORAL PREDICTION

Anonymous authors
Paper under double-blind review

ABSTRACT

Deep learning based approaches have been widely used in various urban spatio-temporal forecasting problems, but most of them fail to account for the unsmoothness issue of urban data in their architecture design, which significantly deteriorates their prediction performance. The aim of this paper is to develop a novel clustered graph transformer framework that integrates both graph attention network and transformer under an encoder-decoder architecture to address such unsmoothness issue. Specifically, we propose two novel structural components to refine the architectures of those existing deep learning models. In spatial domain, we propose a gradient-based clustering method to distribute different feature extractors to regions in different contexts. In temporal domain, we propose to use multi-view position encoding to address the periodicity and closeness of urban time series data. Experiments on real datasets obtained from a ride-hailing business show that our method can achieve 10%-25% improvement than many state-of-the-art baselines.

1 INTRODUCTION

The aim of this paper is to use urban data to study spatio-temporal prediction problems, whose goal is to forecast region-based spatial distribution in the future (Shi & Yeung, 2018; Wang et al., 2019). Recently, region-based spatio-temporal forecasting has been extensively studied with various applications in traffic (Li et al., 2018b), ride-hailing services (Zhang et al., 2018; Li & Zheng, 2019), environment (Liang et al., 2018), resources (Li & Zheng, 2019), and human flows (Wang et al., 2019; Shi et al., 2020), among others. Such spatio-temporal forecasting is crucial for various tasks, such as dispatching and pricing, in urban computing (Zheng et al., 2014). Accurate spatiotemporal forecasting methods may not only lower the barrier for decision making, but also improve the quality of various services including traffic management, transportation, and air quality management. However, achieving accurate prediction represents major challenges for many existing methods due to some difficulties in urban data, such as unsmoothness.

As an illustration, we will show throughout the paper that urban spatiotemporal prediction task suffers from spatial and temporal unsmoothness. Unsmoothness is a common phenomenon in spatial and/or temporal data. The observations in some locations/time-steps differ substantially from the observations in their neighboring locations/time-steps. Representing the spatial or temporal neighborhood[1] of unsmooth region/time-step x as $\mathcal{N}(x)$, the context-aware probability distribution of unsmooth regions/time-steps x_{us} ($x_{us} \in x$), denoted by $P(x_{us}|\mathcal{N}(x_{us}))$, is greatly deviating from the general distribution $P(x|\mathcal{N}(x))$. See a preliminary analysis in Appendix A for details.

For example, rush-hour traffic surge is temporally unsmoothed, while it occurs in many regions in a city. Figure 1 shows potential spatial unsmoothness due to different points
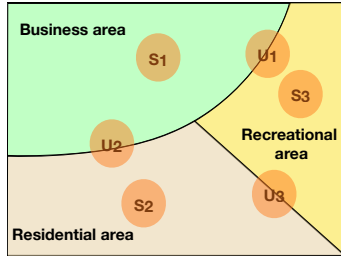

Figure 1: An example of spatial distribution for illustrating spatial smoothness and unsmoothness, where S_1, S_2 and S_3 are smooth function areas and U_1, U_2 and U_3 are on their boundaries.

---

[1]Collection of spatially or temporally close region/timesteps to the centering region/timestep

of interest. Specifically, S_1, S_2 and S_3 denote business, residential, and recreational areas, respectively, whereas U_1, U_2, and U_3 are their boundaries. Traffic observations in the interior areas of S_1, S_2 and S_3 may be quite close to each other, whereas observations along U_1, U_2, and U_3 may have much larger variations. However, the attempt to handling unsmoothness is quite limited both at model and feature levels. Many existing prediction methods share their spatial and temporal feature extractors universally across all time-steps and/or all regions. Thus, it greatly limits the expressiveness of those prediction methods, since they are greatly vulnerable to the presence of unsmoothness in urban data.

In this paper, we develop a novel Clustered Graph Transformer (CGT) framework by integrating Graph Attention Network (GAT) (Veličković et al., 2018) with Transformer (Vaswani et al., 2017) based on a unified attention encoder-decoder architecture (Bahdanau et al., 2015). The GAT and Transformer are effective methods for spatial and temporal feature extraction based on attention mechanism. To handle spatial unsmoothness, we develop a novel Clustered Graph Attention Network (CGAT) by leveraging different graph attention kernels on different regions. The CGAT learns clustering assignments for each region according to their temporal patterns so that regions with different temporal patterns are assigned with different spatial feature extractors. To handle temporal unsmoothness, we propose additivity-preserved multi-view position encoding (MVPE) by characterizing different kinds of temporal relationship including weekly or daily periodicity and temporal closeness (Zhang et al., 2017). In summary, our major contributions are summarized as follows:

- To the best of our knowledge, CGT is the first of its kind in using graph attention network with a transformer under an encoder-decoder architecture for long sequence spatiotemporal forecasting.
- We propose to improve the expressiveness of spatial feature extraction using the clustering technique. We handle the temporal unsmoothness by MVPE, which is a tailored position encoding for urban computing.
- Compared with existing baseline models, CGT achieves improvement ranging from 10% to 25% in spatiotemporal prediction on various tasks, datasets and cities. Error reduction on unsmooth areas dominates this improvement.

2 Methodology

We formalize the learning problem of urban spatiotemporal forecasting and introduce the CGT framework to capture the spatial and temporal dependencies and unsmoothness of urban data.

2.1 Urban spatiotemporal forecasting

We consider urban spatiotemporal forecasting problems in a city. Suppose that the city can be divided into V disjoint regions and we observe temporal information across T time intervals within each region. Our spatio-temporal data is represented as a $|V| \times T$ matrix. As an example, we consider taxi demand forecasting problem and each entry in the matrix represents the total number of taxi orders inside a region within a specific time interval. Our prediction problem is formulated as $f : \mathbb{R}^{|V| \times T_x} \to \mathbb{R}^{|V| \times T_y}$ such that we use the historical data within time period T_x to predict the future trend in time period T_y, that is,

$$\mathbf{X}_{t-T_x+1:t} = [X^{t-T_x+1}, \dots, X^t] \xrightarrow{f(\cdot)} \mathbf{X}_{t+1:t+T_y} = [X^{t+1}, \dots, X^{t+T_y}]. \tag{1}$$

Problem (1) is a *one-step prediction problem* as $T_y = 1$ and a *multi-step prediction problem* as $T_y > 1$. We regard the whole city as a graph with V regions (or vertices), each of which has both demand and supply numbers across T time intervals. Moreover, we construct a set of graph adjacency matrices $\mathbb{G}$ in order to characterize multiple region-wise relationships among different vertices including region-wise distance, POI similarity and road connectivity (Geng et al., 2019).

2.2 Framework overview

Figure 2 shows the overview of the CGT framework. The CGT is an encoder-decoder based architecture. The clustered attention blocks (CABs) and temporal attention blocks (TABs) are stacked
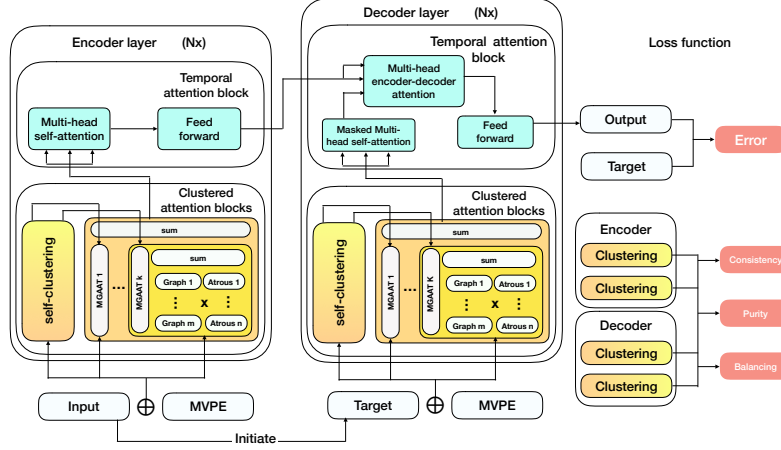
Figure 2: The CGT framework overview.

alternatively in the encoder and decoder. For prediction problem (1), the input tensor to encoder is $\mathbf{X}_{t-T_x+1:t}$. In the training phase, the whole target sequence $\mathbf{X}_{t:t+T_y}$ is input to the decoder and the masked attention controls the visibility of target sequence in each step of decoding. The $\mathbf{X}_t$ is used to initialize the decoder state at the initial decoding step. In the testing phase, at step T_s ($T_s \leq T_y$), the decoder input tensor is $[\mathbf{X}_t, \hat{\mathbf{X}}_{t+1:t+T_s}]$, where $\hat{\mathbf{X}}$ represents predicted values from previous steps. The MVPE is added to input tensors in both encoder and decoder.

Our key novel contribution in CGT lies in the design and use of CAB. The CAB integrates spatial k-clustering, multi-graph ($\mathbb{G}$) and atrous attention ($\mathbb{K}$) together. Each CAB consists of K multi-graph atrous attention networks (MGAAT). Each MGAAT controls spatial feature extraction for one cluster through multi-graphs and multi-atrous kernels by summing up latent features from totally $|\mathbb{G}| \times |\mathbb{K}|$ GATs. The CABs generate soft self-clustering assignment scores for vertices based on their latent features. Different MGAATs are weighted differently on each vertex based on the assignment scores. For temporal feature extraction, we designed multi-view position encoding (MVPE) as supplementary input to encode sequence information from different perspectives. The MVPE helps with the temporal feature extraction in temporal attention block (TAB).

2.3 ADDITIVITY PRESERVED MULTI-VIEW POSITION ENCODING

We design a multi-view position encoding mechanism (MVPE) for urban computing. Figure 3 presents MVPE in details. The position encoding consists of five channels as follows. There are two channels for weekly periodicity given by

$$PE_1(x) = (1 + \sin(2\pi x/7))/2 \quad \text{and} \quad PE_2(x) = (1 + \cos(2\pi x/7))/2.$$

There are two channels for daily periodicity given by

$$PE_3(x) = (1 + \sin(2\pi x))/2 \quad \text{and} \quad PE_4(x) = (1 + \cos(2\pi x))/2.$$

There is one channel for closeness given by

$$PE_5(x) = \exp(-ax^2).$$

The MVPE mechanism inherits two important properties from natural language processing applications. First, multi-view position encoding provides unique identifiers for all time-steps in temporal sequences. For non-recurrent neural network methods, it is critical to use different channels to incorporate some position information into the input. Second, the four periodicity channels based on trigonometric functions maintain their additivity. Although the closeness channel does not maintain additivity, the active time sequence for closeness channel is usually short and concentrated so that it does not incorporate any long-term dependency. Moreover, MVPE encodes similar and correlated time-steps with similar encodings. According to Zhang et al. (2016), when predicting the time series magnitude at a specific time-step, it is critical to consider historical observations at close hours and days before with the same time and weeks before with the same day and the same time.
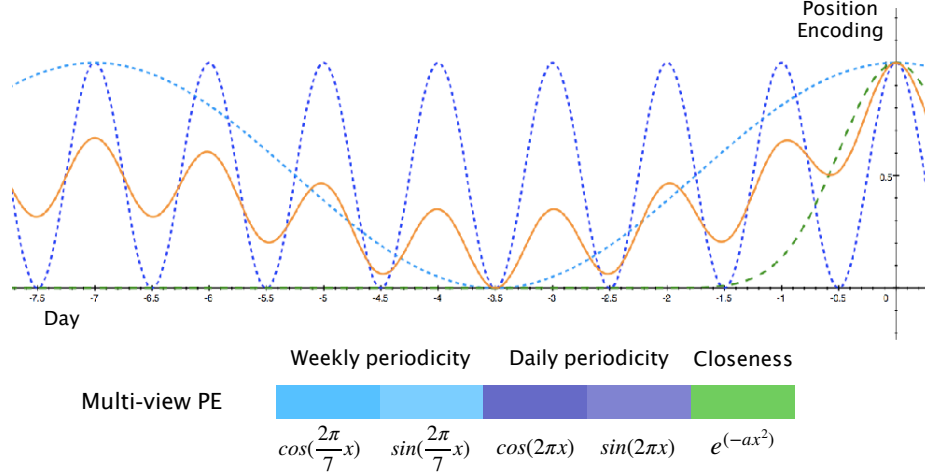
Figure 3: The multi-view position encoding: construction and feature vector layout.

2.4 CLUSTERED ATTENTION BLOCK

We propose the clustered attention block (CAB) for spatial feature extraction. It learns different graph neural network (GNN) kernels for different regions based on a gradient-based self-clustering assignment such that different regions are treated differently in spatial dependency modeling. Within each GNN kernel, we use atrous attention to reduce its computational cost. Moreover, we incorporate the multi-graph technique to delineate multiple region-wise relationships in graph formulation. We name this refined GNN structure as multi-graph atrous attention network (MGAAT). Figure 4 presents an overview of CAB.
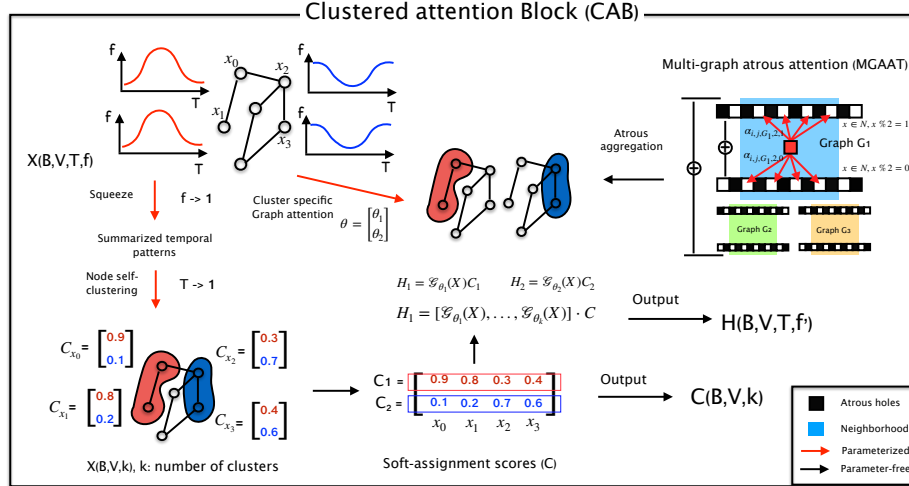

Figure 4: An illustration of the computational flow of clustered attention block.

We discuss several key components of CAB below. First, a vertex-level soft-assignment to K clusters is learnt from the temporal pattern of each vertex:

$$C = \sigma_s(\sigma_r(X_f W_f)_t W_t), \tag{2}$$

where C is the cluster assignment score for each vertex to K clusters. W_f and W_t are parameters for linear layers on the feature mode and temporal mode, respectively, and σ_r and σ_s represent the relu and softmax activation functions, respectively. The feature dimension of input tensor X_f is first squeezed to 1 using W_f, in order to provide summarized temporal pattern at each vertex. The W_t is further applied to the temporal pattern to calculate a $K-$dimensional cluster assignment score.

Second, we use $c_{x_i,k}$ to denote the assignment score of C for assigning vertex x_i to cluster k. Then, C is used to re-weight the latent output by using K MGAATs as follows:

$$h_{x_i} = \sum_{k=0}^{K} \mathcal{G}_{\theta_k}(x_i) c_{x_i,k}, \tag{3}$$

where h_{x_i} is the summed output for each CAB at vertex x_i and $\mathcal{G}_{\theta_k}(x_i)$ is the output for each MGAAT at vertex x_i. Let $\theta_k = (W_k, a_k)$ be the set of all parameters in each MGAAT layer and $\mathcal{N}_{g,i}$ be the neighborhood of the ith vertex on graph g. Each of K MGAATs is based on multiple graphs. The atrous graph attention for vertices i and j on graph g is calculated as

$$\alpha_{i,j,g,s,a} = \frac{\exp(\sigma(a_k^T[W_k h_i || W_k h_j])) I_{s,a}(j)}{\sum_{m \in \mathcal{N}_{g,i}} \exp(\sigma(a_k^T[W_k h_i || W_k h_m])) I_{s,a}(m)}, \tag{4}$$

where σ is the Leakyrelu activation function. $I_{s,a}(i)$ is a masking function for atrous attention with s and a being the atrous stride and the offset, respectively, such that

$$I_{s,a}(j) = \begin{cases} 1 & \text{if } j \bmod s = a; \\ 0 & \text{otherwise.} \end{cases}$$

The output of MGAAT is a combination of GAT on multiple graphs $\mathbb{G}$ given by

$$\mathcal{G}^{(s,a)}(x_i) = \sigma(\sum_{g \in \mathbb{G}} \sum_{j \in \mathcal{N}_{g,i}} \alpha_{i,j,g,s,a} W h_j I_{s,a}(j)). \tag{5}$$

Third, to complete the feature extraction process, we combine s CABs across atrous offset a from 0 to $s-1$ in order to cover the entire neighborhood of each centering vertex. The s atrous attentions could be combined by using either in-layer aggregation given by

$$\mathcal{G}_{\theta_k}(x_i) = \sum_{a=0}^{s-1} \mathcal{G}^{(s,a)}(x_i), \tag{6}$$

or layer stacking given by:

$$\mathcal{G}_{\theta_k}(x_i) = \sigma(\mathcal{G}^{(s,s-1)}(\cdots \sigma(\mathcal{G}^{(s,1)}(\sigma(\mathcal{G}(\mathcal{G}^{(s,0)}(x_i))))))). \tag{7}$$

2.5 TEMPORAL ATTENTION AND TRANSFORMER

The temporal feature is extracted by adapting the multi-head attention model to the temporal mode of spatio-temporal tensor (Vaswani et al., 2017). Detailed information is included in Appendix B.

2.6 OPTIMIZATION OBJECTIVE

The optimization objective of CGT consists of two major components. The first component is the prediction error given by

$$L_{pred} = ||\mathbf{y} - \hat{\mathbf{y}}||_2, \tag{8}$$

where $|| \cdot ||_2$ the standard L_2 norm and $\hat{\mathbf{y}}$ and $\mathbf{y}$ are, respectively, the tensor of predicted values and that of true values.

The second component consists of three constraints for obtaining an optimal vertex cluster schema C. Let the clustering result $C = (C_{b,l,v,k})$ be a tensor of order (B, L, V, K) [2], where B is the batch size, L is the number of all GNN layers, V is the number of vertices, and K is the cluster number. Thus, $C_{b_1,l_1,\cdot,\cdot}$ denotes a $V \times K$ matrix and $C_{b,l,v,\cdot}$ is a $K \times 1$ vector. The three constraints including consistency, purity, and diversity are summarized below.

- Consistency: The clustering assignment is generated through the temporal pattern of each vertex such that C should be temporally (batch) invariant and layer invariant. The loss function for ensuring consistency is defined as

$$L_c = \frac{4}{BL(B-1)(L-1)V^2} \sum_{b_1=1}^{B-1} \sum_{b2=b1+1}^{B} \sum_{l_1=1}^{L-1} \sum_{l_2=l_1+1}^{L} ||C_{b_1,l_1,\cdot,\cdot} - C_{b_2,l_2,\cdot,\cdot}||_2^2. \tag{9}$$

---

[2]There is no constraint on C from different graphs $\mathbb{G}$. We ignore multi-graph here for simplicity.

- Purity: Ideally, each vertex should be only assigned to one cluster. The loss function for encouraging purity is given by

$$L_p = \frac{1}{BLV} \sum_{b=1}^{B} \sum_{l=1}^{L} \sum_{v=1}^{V} (1 - ||C_{b,l,v,\cdot}||_2^2). \quad (10)$$

- Diversity: To balance the cluster size, we define the loss function for ensuring diversity as follows:

$$L_d = \frac{1}{BLV^2} \sum_{b=1}^{B} \sum_{l=1}^{L} ||\sum_{v=1}^{V} C_{b,l,v,\cdot}||_2^2. \quad (11)$$

The overall minimization goal is to minimize the following object function

$$\mathcal{L} = L_{pred} + \alpha(L_c + L_p + L_d), \quad (12)$$

where α is a tuning parameter.

3 RELATED WORK

3.1 SPATIOTEMPORAL DEEP LEARNING

There have been various ways to model the spatial and temporal dependencies with deep neural networks. The combination of CNN and RNN is the most intuitive one (Yao et al., 2018; Zhang et al., 2017; Wang et al., 2017; Liao et al., 2018; Rodrigues et al., 2019). However, CNN-based architectures are unable to handle non-Euclidean region-wise relationships. The STMGCN (Geng et al., 2019), DCRNN (Li et al., 2018b) and GCNN-DDGF (Lin et al., 2018) use ChebNet (Kipf & Welling, 2017) and diffusion convolution to extract spatial features based on rather complex graph representations. The graph attention network (Veličković et al., 2018) is the third generation of spatial modeling, which has more complex structures for discovering region-wise relationships. The ST-MetaNet (Pan et al., 2019) is a representative work of GAT with application in urban computing. In temporal feature extraction, attention-based methods outperform RNNs in terms of both accuracy and efficiency. The ASTGCN (Guo et al., 2019) is an attention-based model on both spatial and temporal domains. The GeoMAN (Liang et al., 2018) further adapts the attention-based model to encoder-decoder architecture for long sequence prediction. However, all existing methods neglect the unsmoothness problem of urban data.

3.2 GRAPH NEURAL NETWORKS

The research works on graph neural networks could be summarized in several categories (Zhou et al., 2018). Spectral graph convolution (Hammond et al., 2011; Kipf & Welling, 2017) defines convolution operator by the eigen-decomposition of the graph laplacian, based on the graph spectral theorem. Non-spectral graph convolution (Duvenaud et al., 2015; Atwood & Towsley, 2016; Hamilton et al., 2017) directly operates the spatial domain by defining a set of neighborhood aggregation and updating rules on vertex-level. Moreover, the gated GNN (Li et al., 2015) leverages the gating technique from LSTM, which provides more complex operations for neighborhood aggregation. GAT (Veličković et al., 2018) is using attention mechanism to discover the vertex-wise similarities in a graph. In urban computing, the intuition is confident that regions are strongly correlated. The GAT might help to discover this intrinsic structure in the region-based spatial distribution.

3.3 VERTEX CLUSTERING AND GRAPH POOLING

Vertex clustering is a frequently used method for graph pooling (Ying et al., 2018), which is a common technique migrated from computer vision. However, the intuition for graph pooling and vertex clustering proposed in this work is different. Graph pooling is to reduce the number of vertices such that vertices in each cluster are regarded sampled into one in the next layer. Downscaling the graph layer would improve model generality and reduce computational cost. The vertex clustering in our approach is to discover a set of vertices sharing similar patterns, which is used for better feature extraction.

3.4 HANDLING UNSMOOTHNESS IN MACHINE LEARNING

Non-local mean methods are proposed for image denoising and restoration by investigating the pixel-level self-similarity in images. Buades et al. (2005) proposed to calculate pixel pair-wise similarity within a large search window. The densities for noisy pixels are interpolated by those similar pixels. Wang et al. (2018),Liu et al. (2018) designed non-local neural networks to incorporate the similar idea in deep learning. However, these non-local mean methods are applied to fix part of the spatial distribution at corrupted areas, which is different from our problem formulation. In time series prediction, Ding et al. (2018) proposed a extreme-value loss (EVL) for extreme event prediction in time series data. Compared with our method, EVL has no model-level effort to extract unsmooth features from data, which totally relies on the success of optimization algorithm.

4 EXPERIMENTS

We conduct experiments on a demand/supply dataset for ride-hailing services in two cities A and B [3] from Jun 2017 to Jun 2019. The demand data is the number of ride-hailing orders in each region within each time interval. The supply data is the summation of online duration for all ride-hailing drivers. The spatial and temporal distribution is sampled and aggregated into 1km×1km map gridding and 30 minutes temporal sampling interval[4]. For both datasets, we cut off the long tail on the 95th quantile and normalize them by min-max normalization. The duration of the dataset is two years, where first 70% is used for training, 10% for validation, and remaining 20% for test. The multi-graph $\mathbb{G}$ involves region-wise relationships including neighborhood, functional similarity, and road connectivity, which are identical to those used in (Geng et al., 2019). The functional similarity graph is binarized on 0.9 so that three graphs have almost equal graph sparsity[5].

4.1 OVERALL PERFORMANCE

In this section, the encoder and decoder both stack 3 CABs and TABs alternately, with 16 hidden states each. The default clustering number is 3, with atrous stride being equal to 2. The number of heads in TAB multi-head attention is set to be 3. The network is optimized by using scheduled Adam on PyTorch (Paszke et al., 2017).

We conduct both one-step prediction and multi-step prediction experiments. To avoid the long sequence problem, which may exhaust computational resource, we sampled 10 input time-steps for each output time-step T_k. The input time-steps include 3 closest time-steps ($T_{k-1}, T_{k-2}, T_{k-3}$), 2 from daily periodicity (T_{k-48}, T_{k-96}) and 1 from weekly periodicity (T_{k-48*7}). For multi-step prediction, the default output length is 8, the encoder input length is 27.

Data	One-step prediction				Multi-step prediction
	Demand		Supply		Demand
City	City A	City B	City A	City B	City A
HA	12.20 / 0.261	12.35 / 0.298	4.14 / 0.184	2.68 / 0.167	18.07 / 0.345
LR	10.61 / 0.247	10.08 / 0.288	3.22 / 0.148	2.12 / 0.143	14.31 / 0.286
XGBoost	10.28 / 0.233	10.25 / 0.268	3.12 / 0.146	2.07 / 0.140	13.03 / 0.240
m-DMVST	9.85 / 0.223	9.45 / 0.259	2.88 / 0.152	1.94 / 0.137	12.22 / 0.270
m-DCRNN	9.59 / 0.217	9.34 / 0.249	2.88 / 0.149	1.97 / 0.148	10.74 / 0.245
ST-MGCN	9.55 / 0.226	9.34 / 0.259	2.85 / 0.136	1.91 / 0.139	12.29 / 0.276
m-GeoMAN	9.97 / 0.232	9.86 / 0.291	2.94 / 0.145	2.00 / 0.138	11.29 / 0.259
m-ASTGCN	10.23 / 0.273	9.48 / 0.252	3.14 / 0.181	1.98 / 0.140	12.66 / 0.262
Our Method	7.29 / 0.209	7.66 / 0.232	2.66 / 0.131	1.73 / 0.124	7.49 / 0.185

Table 1: The error metrics (RMSE/MAPE) based on the demand-supply datasets in two cities.

Baselines are built based on following research works. For the sake of information fairness, all deep learning models are slightly revised to take in multiple graphs.

---

[3] Anonymous for blind review.
[4] Designed according to industrial practices
[5] In city A, it is roughly 12000 edges for 1296 vertices.

- HA, LR and XGBoost: Historical average, linear regression and XGBoost. The model parameters for LR and XGBoost are shared across space and time. XGBoost is implemented using LightGBM (Ke et al., 2017).

- DMVST (Yao et al., 2018): a CNN-LSTM based model. Region-wise relationships are encoded as external inputs.

- DCRNN (Li et al., 2018b) and ST-MGCN (Geng et al., 2019): Both are GCN-RNN based model for spatiotemporal feature extraction. DCRNN is based on encoder-decoder architecture for multi-step traffic prediction.

- GeoMAN (Liang et al., 2018): an attention-based model on spatial and temporal domain, with encoder-decoder architecture.

- ASTGCN (Guo et al., 2019): an attention-based model on spatial and temporal domain. Spatiotemporal feature extracted using GCN and convolution.

Table 1 summarizes the RMSEs and MAPEs of CGT and state-of-the-art baselines. There are few observations from above experiment results. First, the proposed CGT model outperforms all baselines in all prediction tasks by a large margin. Second, all encoder-decoder based models, including m-DCRNN, m-GeoMAN and CGT, perform well in all multi-step prediction tasks.

4.2 ABLATION STUDY AND PARAMETER TEST

In this section, we show the experiment results of CGT on the one-step demand prediction problem in city A with varying model configurations to show the parameter effect. As shown by figure 5, the optimal result is achieved when $\alpha = 0.1$ and $k = 3$. Table 2 shows the model performance when specific component is removed from CGT. The ablation study shows the significance of our novel contribution.
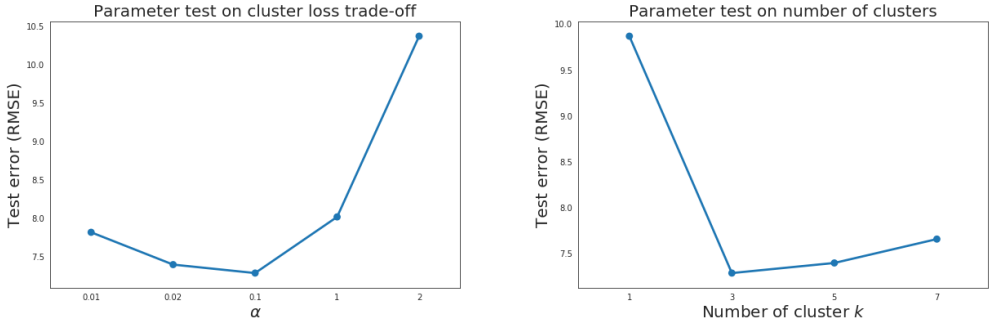

Figure 5: Parameter test for the trade-off parameter α and number of clusters k.

Ablation component	MVPE	Clustering	MVPE and Clustering
RMSE	8.69	9.87	10.11

Table 2: Ablation study for novel components

4.3 MODEL INTERPRETATION

We claim that the prediction error is reduced due to more accurate predictions in spatial and temporal unsmooth areas. To validate this, we explore the relationship between the unsmoothness and the error reduction from a baseline model. The baseline model is designed by removing clustering and MVPE from CGT. Figure 6 shows a positive relationship between unsmoothness and error reduction. Table 3 shows the error reduction from the baseline model on different quantiles of spatial and temporal unsmooth areas. Conclusions could be drawn that CGT could improve the prediction performance, especially in spatial and temporal unsmooth areas by significant margins.
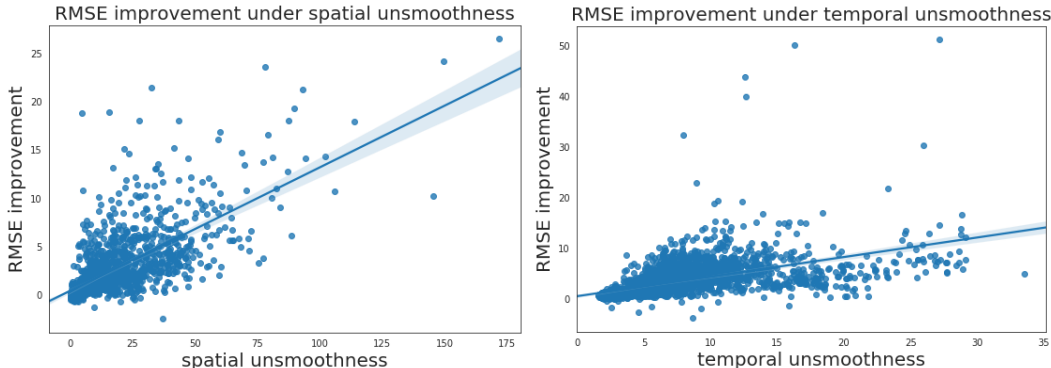
Figure 6: Error reduction and unsmoothness in spatial and temporal domains.

Spatial	Our model	Baseline model	Error reduction	Temporal	Our model	Baseline model	Error reduction
0-50% (smooth)	2.64	3.77	30%	0-50% (smooth)	3.54	4.68	24%
50-75%	6.29	9.30	32%	50-75%	7.08	9.98	29%
75-100% (unsmooth)	11.51	17.65	35%	75-100% (unsmooth)	10.98	16.83	35%

Table 3: Error reduction ratio on different quantiles of unsmoothness in spatial and temporal domains.

5 CONCLUSION AND FUTURE WORK

In this paper, we proposed Clustered Graph-Transformer for spatiotemporal prediction problems in urban computing. To handle the spatial and temporal unsmoothness problem, we use a gradient-based clustering technique in GAT to construct spatial feature extractor. We use MVPE and attention to handle temporal unsmoothness by providing a urban-specific temporal encoding to the temporal mode. The experiment has shown the effectiveness of the proposed model. In the future, we plan to explore long seq2seq problem using atrous transformer (Child et al., 2019) as well as explore the explanation for the attention and clustering assignments.

REFERENCES

James Atwood and Don Towsley. Diffusion-convolutional neural networks. In *Advances in Neural Information Processing Systems*, pp. 1993–2001, 2016.

Dzmitry Bahdanau, Kyunghyun Cho, and Yoshua Bengio. Neural machine translation by jointly learning to align and translate. *International Conference on Learning Representations (ICLR)*, 2015.

Antoni Buades, Bartomeu Coll, and J-M Morel. A non-local algorithm for image denoising. In *2005 IEEE Computer Society Conference on Computer Vision and Pattern Recognition (CVPR'05)*, volume 2, pp. 60–65. IEEE, 2005.

Rewon Child, Scott Gray, Alec Radford, and Ilya Sutskever. Generating long sequences with sparse transformers. *CoRR*, abs/1904.10509, 2019. URL http://arxiv.org/abs/1904.10509.

Daizong Ding, Mi Zhang, Xudong Pan, Min Yang, and Xiangnan He. Modeling extreme events in time series prediction. In *Advances in Neural Information Processing Systems*, 2018.

David K Duvenaud, Dougal Maclaurin, Jorge Iparraguirre, Rafael Bombarell, Timothy Hirzel, Alán Aspuru-Guzik, and Ryan P Adams. Convolutional networks on graphs for learning molecular fingerprints. In *Advances in neural information processing systems*, pp. 2224–2232, 2015.

Xu Geng, Yaguang Li, Leye Wang, Lingyu Zhang, Qiang Yang, Jieping Ye, and Yan Liu. Spatiotemporal multi-graph convolution network for ride-hailing demand forecasting. In *Proceedings of the AAAI Conference on Artificial Intelligence*, volume 33, pp. 3656–3663, 2019.

Shengnan Guo, Youfang Lin, Ning Feng, Chao Song, and Huaiyu Wan. Attention based spatial-temporal graph convolutional networks for traffic flow forecasting. In *Proceedings of the AAAI Conference on Artificial Intelligence*, volume 33, pp. 922–929, 2019.

Will Hamilton, Zhitao Ying, and Jure Leskovec. Inductive representation learning on large graphs. In *Advances in Neural Information Processing Systems*, pp. 1024–1034, 2017.

David K Hammond, Pierre Vandergheynst, and Rémi Gribonval. Wavelets on graphs via spectral graph theory. *Applied and Computational Harmonic Analysis*, 30(2):129–150, 2011.

Guolin Ke, Qi Meng, Thomas Finley, Taifeng Wang, Wei Chen, Weidong Ma, Qiwei Ye, and Tie-Yan Liu. Lightgbm: A highly efficient gradient boosting decision tree. In *Advances in Neural Information Processing Systems*, pp. 3146–3154, 2017.

Thomas N Kipf and Max Welling. Semi-supervised classification with graph convolutional networks. *International Conference on Learning Representations (ICLR)*, 2017.

Qimai Li, Zhichao Han, and Xiao-Ming Wu. Deeper insights into graph convolutional networks for semi-supervised learning. In *Proceedings of the AAAI Conference on Artificial Intelligence*, volume 33, pp. 3538–3545, 2018a.

Yaguang Li, Rose Yu, Cyrus Shahabi, and Yan Liu. Diffusion convolutional recurrent neural network: Data-driven traffic forecasting. *International Conference on Learning Representations (ICLR)*, 2018b.

Yexin Li and Yu Zheng. Citywide bike usage prediction in a bike-sharing system. *IEEE Transactions on Knowledge and Data Engineering*, 2019.

Yujia Li, Daniel Tarlow, Marc Brockschmidt, and Richard Zemel. Gated graph sequence neural networks. *arXiv preprint arXiv:1511.05493*, 2015.

Yuxuan Liang, Songyu Ke, Junbo Zhang, Xiuwen Yi, and Yu Zheng. Geoman: Multi-level attention networks for geo-sensory time series prediction. In *IJCAI*, pp. 3428–3434, 2018.

Binbing Liao, Jingqing Zhang, Ming Cai, Siliang Tang, Yifan Gao, Chao Wu, Shengwen Yang, Wenwu Zhu, Yike Guo, and Fei Wu. Dest-resnet: A deep spatiotemporal residual network for hotspot traffic speed prediction. In *2018 ACM Multimedia Conference on Multimedia Conference*, pp. 1883–1891. ACM, 2018.

Lei Lin, Zhengbing He, and Srinivas Peeta. Predicting station-level hourly demand in a large-scale bike-sharing network: A graph convolutional neural network approach. *Transportation Research Part C: Emerging Technologies*, 97:258–276, 2018.

Ding Liu, Bihan Wen, Yuchen Fan, Chen Change Loy, and Thomas S Huang. Non-local recurrent network for image restoration. In *Advances in Neural Information Processing Systems*, pp. 1673–1682, 2018.

Zheyi Pan, Yuxuan Liang, Weifeng Wang, Yong Yu, Yu Zheng, and Junbo Zhang. Urban traffic prediction from spatio-temporal data using deep meta learning. In *Proceedings of the 25th ACM SIGKDD International Conference on Knowledge Discovery & Data Mining*, pp. 1720–1730. ACM, 2019.

Adam Paszke, Sam Gross, Soumith Chintala, Gregory Chanan, Edward Yang, Zachary DeVito, Zeming Lin, Alban Desmaison, Luca Antiga, and Adam Lerer. Automatic differentiation in pytorch. 2017.

Filipe Rodrigues, Ioulia Markou, and Francisco C Pereira. Combining time-series and textual data for taxi demand prediction in event areas: A deep learning approach. *Information Fusion*, 49: 120–129, 2019.

Pavel Senin. Dynamic time warping algorithm review. *Information and Computer Science Department University of Hawaii at Manoa Honolulu, USA*, 855(1-23):40, 2008.

Hongzhi Shi, Quanming Yao, Qi Guo, Yaguang Li, Lingyu Zhang, Jieping Ye, Yong Li, and Yan Liu. Predicting origin-destination flow via multi-perspective graph convolutional network. In *2020 IEEE 36th International Conference on Data Engineering (ICDE)*, 2020.

Xingjian Shi and Dit-Yan Yeung. Machine learning for spatiotemporal sequence forecasting: A survey. *arXiv preprint arXiv:1808.06865*, 2018.

Ashish Vaswani, Noam Shazeer, Niki Parmar, Jakob Uszkoreit, Llion Jones, Aidan N Gomez, Łukasz Kaiser, and Illia Polosukhin. Attention is all you need. In *Advances in neural information processing systems*, pp. 5998–6008, 2017.

Petar Veličković, Guillem Cucurull, Arantxa Casanova, Adriana Romero, Pietro Lio, and Yoshua Bengio. Graph attention networks. *International Conference on Learning Representations (ICLR)*, 2018.

Dong Wang, Wei Cao, Jian Li, and Jieping Ye. Deepsd: supply-demand prediction for online car-hailing services using deep neural networks. In *2017 IEEE 33rd International Conference on Data Engineering (ICDE)*, pp. 243–254. IEEE, 2017.

Senzhang Wang, Jiannong Cao, and Philip S Yu. Deep learning for spatio-temporal data mining: A survey. *arXiv preprint arXiv:1906.04928*, 2019.

Xiaolong Wang, Ross Girshick, Abhinav Gupta, and Kaiming He. Non-local neural networks. In *Proceedings of the IEEE Conference on Computer Vision and Pattern Recognition*, pp. 7794–7803, 2018.

Huaxiu Yao, Fei Wu, Jintao Ke, Xianfeng Tang, Yitian Jia, Siyu Lu, Pinghua Gong, Jieping Ye, and Zhenhui Li. Deep multi-view spatial-temporal network for taxi demand prediction. In *Thirty-Second AAAI Conference on Artificial Intelligence*, 2018.

Zhitao Ying, Jiaxuan You, Christopher Morris, Xiang Ren, Will Hamilton, and Jure Leskovec. Hierarchical graph representation learning with differentiable pooling. In *Advances in Neural Information Processing Systems*, pp. 4800–4810, 2018.

Junbo Zhang, Yu Zheng, Dekang Qi, Ruiyuan Li, and Xiuwen Yi. Dnn-based prediction model for spatio-temporal data. In *Proceedings of the 24th ACM SIGSPATIAL International Conference on Advances in Geographic Information Systems*, pp. 92. ACM, 2016.

Junbo Zhang, Yu Zheng, and Dekang Qi. Deep spatio-temporal residual networks for citywide crowd flows prediction. In *Thirty-First AAAI Conference on Artificial Intelligence*, 2017.

Lingyu Zhang, Wei Ai, Chuan Yuan, Yuhui Zhang, and Jieping Ye. Taxi or hitchhiking: Predicting passenger's preferred service on ride sharing platforms. In *The 41st International ACM SIGIR Conference on Research & Development in Information Retrieval*, pp. 1041–1044. ACM, 2018.

Yu Zheng, Licia Capra, Ouri Wolfson, and Hai Yang. Urban computing: concepts, methodologies, and applications. *ACM Transactions on Intelligent Systems and Technology (TIST)*, 5(3):38, 2014.

Jie Zhou, Ganqu Cui, Zhengyan Zhang, Cheng Yang, Zhiyuan Liu, Lifeng Wang, Changcheng Li, and Maosong Sun. Graph neural networks: A review of methods and applications, 2018.

A PRELIMINARY ANALYSIS

In this section, we conduct a preliminary error analysis for a baseline GNN+RNN based model on spatial and temporal unsmooth areas in order to prove our assumptions and motivate our design methodology.

For input spatial temporal signal X, denote X_s and X_t as its spatial and temporal modes, respectively, and L as the graph laplacian matrix for spatial distribution. The $\mathcal{L}$ is the loss metric. The spatial and temporal unsmoothnesses could be represented by the difference between a convoluted value and its true value. We define the spatial convolution kernel as αL, which is a linear combination of the features from all neighboring locations. The temporal convolution kernel is defined as W_t*, which is a 1d convolution along temporal mode. The spatial and temporal unsmoothnesses are calculated as $\phi_s = \mathcal{L}(X, \alpha L X_s)$ and $\phi_t = \mathcal{L}(X, W_t * X_t)$, respectively. The α and W_t are optimized using the same training set as the baseline model. Spatial and temporal areas with larger unsmoothness means that they are hard to be represented by using a linear combination of observations in neighboring locations.
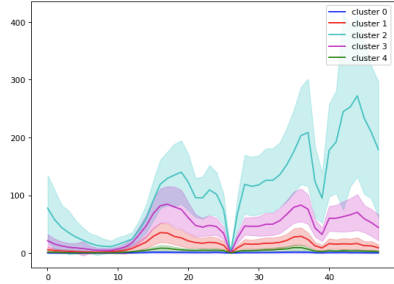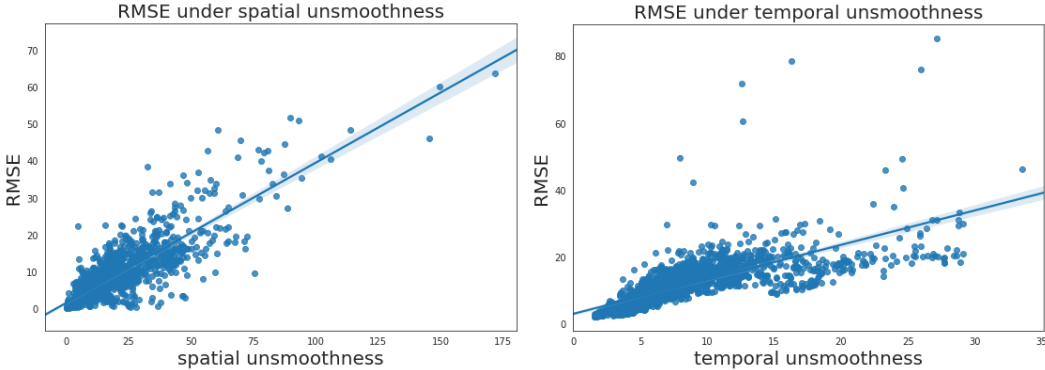

Figure 7: The averaged 24 hour temporal pattern for regions in each cluster, shaded within 1 standard deviation.

(a) Positive relationship between spatial unsmoothness (X) and prediction error (Y) for the baseline model.

(b) Positive relationship between temporal unsmoothness (X) and prediction error (Y) for the baseline model.

Figure 8: Baseline prediction error and unsmoothness

Figure 8 shows the positive relationship between baseline prediction error and spatial/temporal unsmoothness. There are several reasons for this. First, the expressiveness of GNNs are limited. Using ChebNet as an example, it treats all neighbors in one convolution kernel homogeneously and shares its weighted transformation on feature dimension to all neighboring vertices. Thus, ChebNet lacks discriminativity within the neighborhood. Li et al. (2018a) also proves that the usage of laplacian smoothing will cause serious problem in deep-stacked GCN models. Second, spatial feature extractors are shared among all regions, that is, it is assumed that spatial feature extraction rule is universally applied to the whole city. In Figure 7, we clustered the regions in the city into 5 clusters according to their similarities by using DTW (Senin, 2008) of temporal pattern in a short snippet and print averaged 24 hour temporal pattern for them. The clustering result shows that the magnitudes for regions from different clusters are different with high confidence. The overall temporal patterns for different clusters are quite diverse.

B   CALCULATION FOR TEMPORAL ATTENTION IN TRANSFORMER

The temporal attention is calculated as follows:

$$Attn(Q, K, V) = softmax(\frac{QK^T}{\sqrt{d_k}})V,$$

where QK^T is a self-attention to represent relationships among different time-steps. Such relationship is further applied on V by transforming its temporal mode.

The feed forward layer is a linear transformation on the feature mode as follows:

$$H_{ffn}(X) = \sigma_r(X_f W_f).$$

12

In encoder, the self-attention is used to discover temporal dependencies in the latent feature vector h such that the attention is defined as

$$Q = hW_q, K = hW_k, \text{ and } V = hW_v. \tag{13}$$

In decoder, the self-attention performs similarly, but a mask is applied on the input sequence so that the feature extraction at time t could not view the temporal features later than it. The mask is implemented by an upper triangular matrix. The encoder-decoder attention transforms the temporal mode of decoder latent feature based on temporal dependencies from the encoder as follows:

$$Q = h_{enc}W_q, K = h_{enc}W_k, \text{ and } V = hW_v, \tag{14}$$

where h is the decoder latent feature vector from previous decoder layers and h_{enc} is the encoder feature vector which denotes the encoder state. In this application, the initial state for the decoder input sequence (target sequence) is copied from the last time-step of the input sequence.

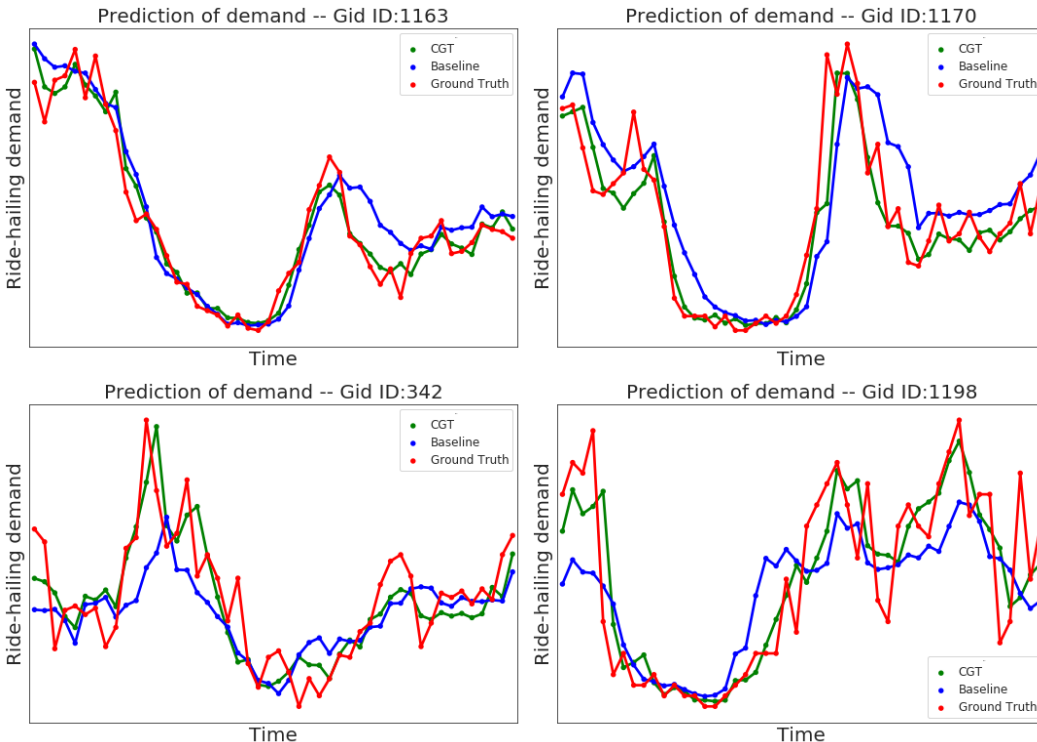## C VISUALIZATION FOR PERFORMANCE ON TEMPORAL UNSMOOTHNESS

Figure 9: Plot 24-hour region demand values to compare ground truth with prediction result of CGT and baseline

Figure 9 shows the comparison between ground truth and machine learning models based on 24-hour ride-hailing demand values in selected regions. According to the visualization, CGT model is more close to ground truth, especially in those temporal unsmoothed areas.